CONAENDI&IEV2020 – 000

Increasing temperature as function of stress amplitudes at ultrasonic fatigue: what is it telling us?

T.L. Castro[1], H.K. Ambo [1], R. Lazzarotto[1], M.V. Pereira[1], S. B. Peripolli[2], M.G.B. Lima[2], V.H. de A. Almeida[2]

Trabalho apresentado durante o XXXVIII – Congresso Nacional de Ensaios Não Destrutivos e Inspeção.
22ª IEV – Conferencia Internacional sobre Evaluación de Integridad y Extensión de Vida de Equipos Industriales.

Abstract

Structural components are currently expected to endure beyond 10^7 loading cycles. Ultrasonic fatigue testing equipment operating in $20\ kHz$ have managed to significantly reduce laboratory tests duration, allowing one to reach $10^7 - 10^{12}$ cycles in a much shorter time when compared to regular fatigue testing systems. However, specimens subjected to ultrasonic fatigue loadings have presented a significant temperature raise during the tests. In order to monitor specimen temperature, a thermographic inspection was carried out during experiments. It was possible to identify different temperature profiles relative to the applied stress amplitudes as well as the temperature distribution within the specimen itself.

Keywords: very high-cycle fatigue (VHCF), $20\ KHz$ fatigue testing system, temperature raise, first and second temperature plateau.

1. Introduction

Fatigue is the most usual failure mechanism in engineering, caused by the exposure in time of the mechanical component to oscillating loading conditions, resulting in fatigue crack nucleation followed by propagation. The comprehension of this phenomenon is crucial to the in-service lifetime prediction of structural components subjected to such loadings. Wöhler S-N curves (stress – number of cycles) relate the number of cycles to failure with the stress amplitudes to which the material is subjected, and such curves are obtained experimentally from fatigue experiments. Conventional S-N curves englobe both low-cycle and high-cycle fatigue regimes, LCF and HCF respectively.

---

1 Pontifícia Universidade Católica do Rio de Janeiro – PUC-Rio.
2 SENAI IST Solda.

In LFC regime, the specimen is subjected to higher stress amplitudes, and therefore withstands fatigue loadings for shorter-periods, ultimately failing upon a smaller number of cycles – typically under 10^4 cycles. In HCF regime, on the other hand, the expected number of cycles to failure is significantly higher as stress loadings are considerably smaller. Under these conditions, specimens could experiment a fatigue-lives as far as 10^7 cycles [1].
As stress loading amplitudes are progressively reduced, the S-N curve presents an asymptotic behaviour towards a specific stress amplitude value known as the endurance limit, a stress amplitude value below which, up until recently, the mechanical component was theoretically expected to present infinite fatigue-life, i.e. the mechanical component was expected to endure fatigue loadings indefinitely without presenting failure. However, due to technological advancements, it has been revealed that fatigue-life can exceed the high-cycle fatigue regime beyond 10^7 loading cycles, making ways to the development of the new concept of very high-cycle fatigue (VHCF) [2-4].
Ultrasonic fatigue experiments revealed a significant temperature increase within each test, establishing a certain temperature-evolving pattern as function of time, as previous studies have also pointed out [5-7]. Therefore, a non-destructive temperature inspection method such as infrared thermography, which is a well-established technique, can be used for temperature monitoring as fatigue experiments are carried out.

2. Very high cycle fatigue

Examples of fatigued mechanical components can easily be found in the several different industrial segments such as automotive, railroad, airline and aerospace as they all design their projects expecting mechanical components to be able to endure long fatigue-lives.
In this context, fatigue experiments that manage to reach 10^{12} cycles are fundamental for the development of components such as turbine axles, crankshafts, bearings among others. Broadly speaking, very high cycle fatigue testing is fundamental to each project design that expects its final product to withstand beyond 10^7 loading cycles.
Very high cycle fatigue studies have contributed to extend the S-N, which is now inclusive to all fatigue cycle regimes as presented in Fig. 1 [3].

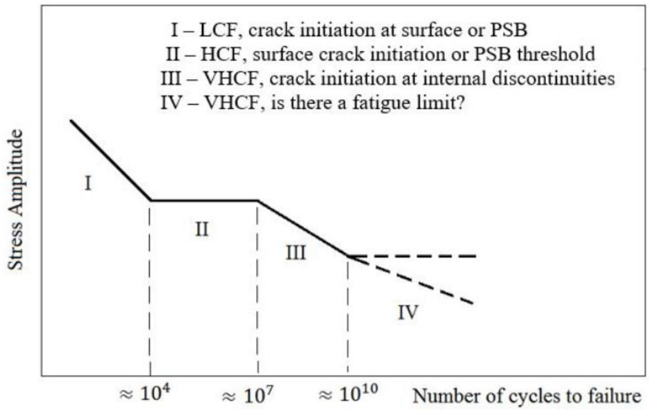

Figure 1: S-N curve including LCF, HCF and VHCF regimes [3]

3. Thermography

In order to detect the temperature variation throughout the longitudinal length of a given material, the thermography technique requires the use of a thermographic camera, equipped with a sensor responsible for detecting the infrared radiation emitted from the specimen. Such radiation is converted into electrical signal and compared to a calibration curve, yielding the temperature data. The output is translated into a thermographic map, which is a digital image discriminating the different temperatures registered in the inspected surface where every pixel corresponds to a given temperature relative to a single surface point of the specimen [8].
There are two basic infrared thermography applications: passive and active thermography. In passive mode, the external excitation source is dismissed as thermal differences of the in-service material are detectable by the infrared sensor. In active mode, the use of an external heat source is required as the heating or cooling of the specimen the main mechanisms capable of producing significant temperature differences [9, 10].
Among many applications in several industrial segments, the use of thermographic cameras on applied research on fatigue has become increasingly common. This can be explained due to the fact that metallic components, when subjected to cyclic loading values close to or just above the fatigue endurance limit, present a sudden increase in temperature, which can be itself an indicative of a fatigue-related phenomenon [11].

4. Materials and methods

4.1 Materials

Two different materials were used, being the first a steel for offshore applications and the second was a regular commercially available SAE 1020. The mechanical properties as well as the chemical compositions are available in Table 1 and Table 2.

Table 1: Mechanical properties of the steels

Mechanical properties		
	Offshore application steel (OAS)	**SAE 1020**
$\boldsymbol{\sigma_u}\ [\boldsymbol{MPa}]$	890	420
$\boldsymbol{\sigma_y}\ [\boldsymbol{MPa}]$	790	350
$\boldsymbol{E}\ [\boldsymbol{GPa}]$	210	205
$\boldsymbol{\rho}\ [\boldsymbol{g/cm^3}]$	7,87	7,87

Table 2 – Chemical composition of the steels

Chemical composition (% wt)									
	C	Mn	Cr	Ni	Mo	V	Ti	P	S
OAS	0.22	1.0	1.1	0.6	0.3	0.07	0.01	–	–
SAE 1020	0.17– 0.23	0.3– 0.6	–	–	–	–	–	< 0.04	< 0.05

In order to obtain better precision while monitoring the temperature, a black coating spray jet paint was applied to the specimens raising the emissivity to 0.93. The spray jet is commercially available and resistant to high temperatures ($600\ °C$) and has in its composition silicone resin, acrylic resin, aluminium, mineral charges, silicon dioxide, aromatic and aliphatic hydrocarbon as well as propellant gas (butane/propane).
The emissivity was verified by comparing the obtained thermography data to measurements using a manual thermocouple contact system.

4.2 Thermographic analysis

The used camera was a FLIR A655SC on passive mode, to which was coupled an infrared lens IR with focal distance of $f = 41.3\ mm\ (15°\ FOV)$, as illustrated in Fig. 2.

Figure 2: Illustration of the thermographic camera

Table 3 presents the parameters relative to both ambient conditions at the moment that the fatigue tests were carried out and passive thermography configurations.

Table 3: Parameters of the fatigue experiments

Experimental test parameters	
Distance of camera to specimen	$0.5\ m$
Room temperature	$\sim 20\ °C$
Emissivity	0.93
Frames per second	100
Temperature range settings	$-40\ to\ 150\ °C;\ \ 100\ to\ 650\ °C;\ \ 300\ to\ 2000\ °C$

4.3 Fatigue testing system and specimen geometry

Experiments were carried out on a Shimadzu USF-2000A, the only fatigue testing system in Latin America capable of subjecting specimens to fully reversed fatigue loadings at very high frequency ($20\ kHz$). Specimen's dimensions must be designed in order to meet the desired resonance frequency, which is dependent on physical and material properties. The differences in specimen geometry are presented in Fig. 3 and in Fig. 4.

Figure 3: Generic sample of specimen geometry used in ultrasonic fatigue testing

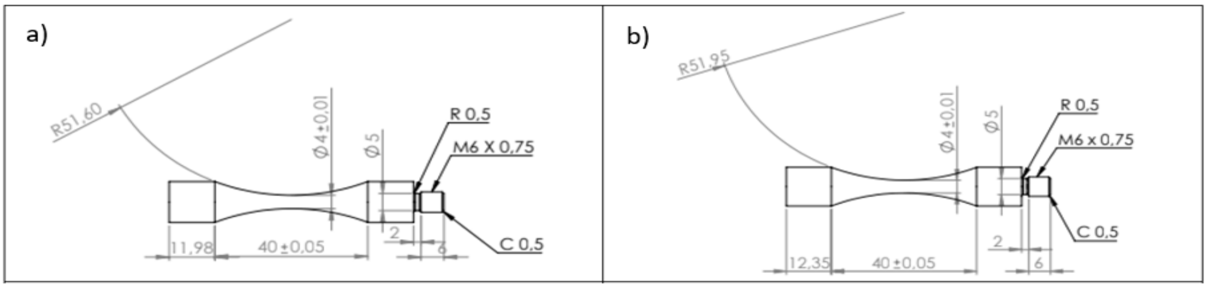

Figure 4: (a) Specimen's dimensions for SAE 1020; (b) Specimen's dimensions for the offshore application steel

4.4 Stress amplitude loadings and temperature monitoring

The stress amplitude loadings applied in the fatigue experiments were chosen relative to the ultimate tensile stress σ_u. The applied stress amplitudes aimed for $0.45\,\sigma_u$, $0.475\,\sigma_u$ and $0.50\,\sigma_u$ for both materials, each one of them having its own particular σ_u. An additional test was carried out aiming to subject the SAE 1020 steel to $0.4\,\sigma_u$.
The real applied stresses were similar to the designed stresses and are presented in Table 4.

Table 4: Loadings applied in the ultrasonic fatigue experiments

Offshore application steel	–	$0.45\,\sigma_u$	$0.472\,\sigma_u$	$0.483\,\sigma_u$
SAE 1020	$0.393\,\sigma_u$	$0.44\,\sigma_u$	$0.476\,\sigma_u$	$0.50\,\sigma_u$

Stress amplitude loadings are to be kept under the yield stress in order to assure the elastic nature of the experiment, minding the fact that the endurance limit could be anywhere within in a range of $0.35\,\sigma_u$ and $0.50\,\sigma_u$. Three offshore application steel and two SAE 1020 specimens were tested in order to obtain experimental data, and stress amplitudes were set between $0.40\,\sigma_u$ and $0.50\,\sigma_u$. Temperature behaviour was monitored until the specimen presented temperature stabilisation, which occurred around 10^7 cycles. After stabilising, the test was interrupted for the specimen cool down. The procedure should be restarted applying a higher stress amplitude as soon as the specimen once again reached room temperature. Should material failure occur, the specimen was to be replaced and the experiment would be reinitiated from the point where it was interrupted.

5. Results and discussion

In Fig. 5, the temperature vs. number of cycle curves relative to four different loading conditions applied to SAE 1020 are presented. The first applied stress amplitude of $165\ MPa$ is equivalent to $0.40\ \sigma_u$. The specimen presented initial temperature of $24\ °C$, revealing a slight increase of temperature at 1.8×10^5 cycles, reaching a maximum temperature of $36.8\ °C$. The curve relative to the stress amplitude of $185\ MPa$, i.e. $\sigma_a = 0.44\ \sigma_u$, also presented a similar behaviour, reaching a maximum temperature of $47\ °C$. Nevertheless, the next specimen which was subjected to stress amplitudes of $200\ MPa$, i.e. $\sigma_a = 0.476\ \sigma_u$, presented not only the same initial temperature increase as the previous two, but also presented a second increase in temperature a second plateau. The initial temperature was registered at $22\ °C$ and the specimen also presented the expected minor increase of temperature, followed by stabilisation at 2.8×10^5 cycles. At 2×10^7 cycles, however, a sudden increase of temperature was revealed, reaching a temperature of $388.15\ °C$. After the peak, temperature remains oscillating between $350\ °C$ and $380\ °C$, characterising a second temperature plateau. Once applied the next stress amplitude level of $210\ MPa$, i.e. $\sigma_a = 0.50\ \sigma_u$, the initial temperature was registered at $27\ °C$, and once again the specimen presented the expected slight increase of temperature, stabilising at the first temperature plateau. At 3×10^6 cycles there was an abrupt temperature increase reaching a peak of $499.3\ °C$, followed by stabilisation at elevated temperatures. The experiment was interrupted at 2×10^7 cycles.

As previously described in the literature [5-7], the high temperature peaks exceed the glass-transition temperature (T_g) of the polymeric matrix-based spray jet paint. This reduces the emissivity, explaining why the peaks are followed by temperature drops before stabilising on the second plateau. The final part of the curve indicates a temperature drop meaning that the camera continued to monitor the temperature for some time even after the experiment was interrupted.

In Fig. 6, the temperature vs. number of cycle curves relative to three different loading conditions applied to the offshore application steel are presented. The first applied stress amplitude of $\sigma_a = 400\ MPa$, i.e. equivalent to $0.45\ \sigma_u$. The initial temperature of the specimen was $23\ °C$, which once again revealed the sudden temperature raise at 4.5×10^5 cycles, reaching a maximum temperature value of $240.05\ °C$. The experiment was interrupted just before 10^7 cycles, revealing no evidence of change in the temperature behaviour. The second loading condition relative to this material subjected the specimen to $\sigma_a = 420\ MPa$, i.e. $0.472\ \sigma_u$. The initial temperature increase raised the temperature from $25\ °C$ to $200\ °C$, followed by temperature stabilisation. By 4×10^6 cycles, due to another abrupt increase of temperature, it was possible to register $513\ °C$. The last tested loading condition where $\sigma_a = 430\ MPa$, i.e. $0.483\ \sigma_u$, even though the specimen was initially at room temperature, the first registered temperature in the experiment was of approximately $100\ °C$, meaning that the increase of temperature was so abrupt that the infrared camera did not manage to detect the initial lower temperatures. By 1.7×10^5 cycles, there was another increase, reaching a maximum temperature of $554.39\,°C$. At 8×10^6 cycles, the experiment was automatically interrupted probably due to the fact that the fatigue system may have identified specimen failure. Both $420\,MPa$ and $430\,MPa$ curves reveal the temperature increases followed by plateaus, indicating temperature stabilisation.

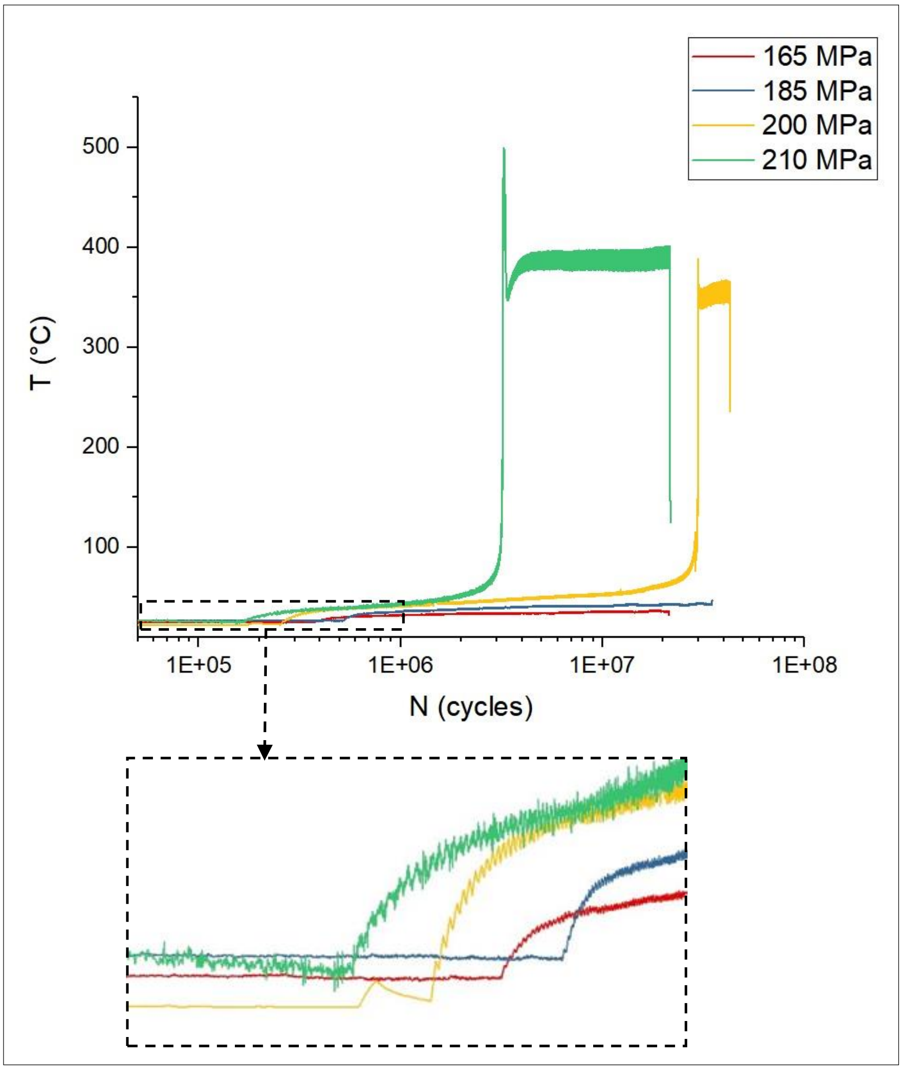

Figure 5: T-N curve for SAE 1020.

When subjected to stress amplitudes loadings greater or approximately equal to $\sigma_a \approx 0.47\,\sigma_u$, both steels presented an abrupt increase of temperature followed by a temperature plateau. According to previous studies [5-7], the first plateau level indicates a possible fatigue crack nucleation stage. The second temperature raise could be mean that the material has exhausted its nucleation stage experiencing fatigue crack growth. Temperature remains on high levels until fatigue crack takes place.

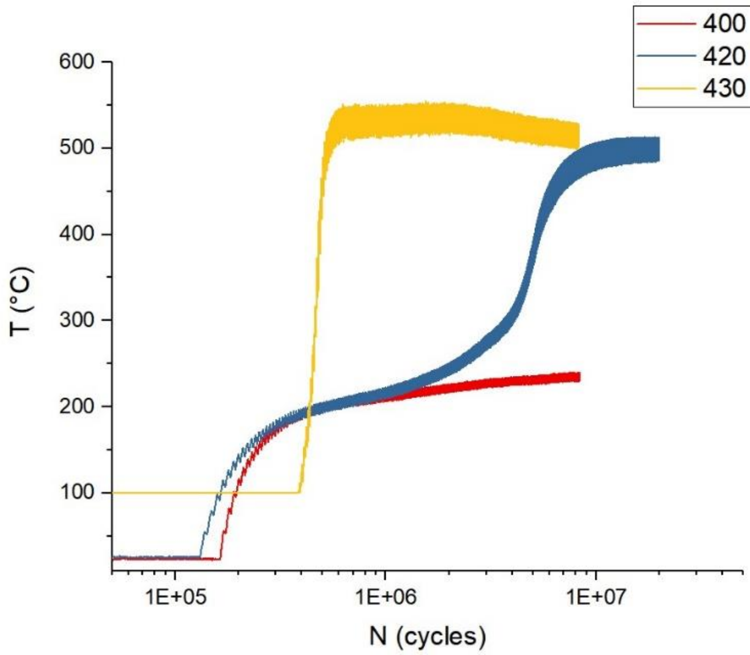

Figure 6: T-N curve for the offshore application steel.

6. Conclusions

- Throughout ultrasonic fatigue experiments, temperature levels are a function of the stress loading levels to which the specimen is subjected. Higher stress amplitudes yield higher temperatures.
- Both materials presented temperature stabilisation by 10^7 cycles.
- For stress loading greater or approximately equal to $\sigma_a \approx 0.47\, \sigma_u$, two different temperature plateaus were revealed, as well as a temperature peak preceding the second plateau.
- The offshore application steel presented higher temperatures compared to commercially available SAE 1020, as it has been subjected to higher stress loadings.
- The first temperature plateau may be related to crack nucleation while second temperature plateau my be related to crack propagation.

7. Acknowledgements

This research (work) was developed within the scope of the Research and Technological Development of the Brazilian Electric Energy Sector Program regulated by ANEEL, with the support of the Eneva Companies - Pecém II Energy Generation S.A., Itaqui Energy Generation

S.A., Parnaíba Energy Generation and Commercialization S.A. and Parnaíba II Energy Generation S.A.
This work was also supported by SENAI ISI Inspection and Integrity for all conducting infrared thermography tests.

8. References

[1] S. Suresh, Fatigue of Materials, New York: Cambridge University Press, 1998.
[2] Bathias, C., Paris, P. C., Gigacycle Fatigue in Mechanical Practice, (2005), Marcel Dekker, New York.
[3] M.C. Teixeira, Comportamento do Aço DIN 34CrNiMo6 em Fadiga de Altíssimo Ciclo, Dissertação de Mestrado, PUC-Rio, 2018.
[4] M.V. Pereira, M.C. Teixeira, F.A. Darwish. Correlation between fractographic aspects and stress intensity factor in very high cycle fatigue, Procedia Structural Integrity, 17 (2019), pp 105-114.
[5] V. Crupi, G. Epasto, E. Guglielmino, G. Risitano, Analysis of temperature and fracture surface of AISI4140 steel in very high cycle fatigue regime, Theoretical and Applied Fracture Mechanics, Vol. 80, Part A, 2015, pp. 22-30.
[6] W. Yang, X. Guo, Q. Guo, J. Fan, Rapid evaluation for high-cycle fatigue reliability of metallic materials through quantitative thermography methodology, International Journal of Fatigue, Vol. 124, 2019, pp. 461-472.
[7] X.G. Wang, V. Crupi, X.L. Guo, Y.G. Zhao, Quantitative Thermographic Methodology for fatigue assessment and stress measurement, International Journal of Fatigue, Vol. 32, Issue 12, 2010, pp. 1970-1976
[8] X. Maldague, Theory and practice of infrared technology for nondestructive testing, John Wiley & Sons, New York 2001.
[9] N. Vilardo, Utilização da técnica de termografia e de simulação computacional para detecção de defeitos em compósitos de fibra de carbono, Dissertação de Mestrado, COPPE/UFRJ, 2018.
[10] R. Montanini, Quantitative determination of subsurface defects in a reference specimen made of Plexiglas by means of lock-in and pulse phase infrared thermography", Infrared Physics & Technology, v. 53, pp. 363-371, 2010.
[11] P.D. Stanley, W.K. Chan, Quantitative stress analysis by means of the thermoelastic effect",J. Strain Analysis, vol. 20, pp. 129-137, 1985.